EUKARYOTIC CELL, July 2011, p. 932–944 Vol. 10, No. 7
1535-9778/11/$12.00 doi:10.1128/EC.05005-11

Live Imaging of Disseminated Candidiasis in Zebrafish Reveals Role of Phagocyte Oxidase in Limiting Filamentous Growth▽†‡

Kimberly M. Brothers,[1,2] Zachary R. Newman,[1] and Robert T. Wheeler[1,2]*

Department of Molecular and Biomedical Sciences[1] and Graduate School of Biomedical Sciences,[2] University of Maine, Orono, Maine 04469

Received 9 February 2011/Accepted 26 April 2011

Candida albicans **is a human commensal and a clinically important fungal pathogen that grows in both yeast and hyphal forms during human infection. Although *Candida* can cause cutaneous and mucosal disease, systemic infections cause the greatest mortality in hospitals. Candidemia occurs primarily in immunocompromised patients, for whom the innate immune system plays a paramount role in immunity. We have developed a novel transparent vertebrate model of candidemia to probe the molecular nature of *Candida*-innate immune system interactions in an intact host. Our zebrafish infection model results in a lethal disseminated disease that shares important traits with disseminated candidiasis in mammals, including dimorphic fungal growth, dependence on hyphal growth for virulence, and dependence on the phagocyte NADPH oxidase for immunity. Dual imaging of fluorescently marked immune cells and fungi revealed that phagocytosed yeast cells can remain viable and even divide within macrophages without germinating. Similarly, although we observed apparently killed yeast cells within neutrophils, most yeast cells within these innate immune cells were viable. Exploiting this model, we combined intravital imaging with gene knockdown to show for the first time that NADPH oxidase is required for regulation of *C. albicans* filamentation *in vivo*. The transparent and easily manipulated larval zebrafish model promises to provide a unique tool for dissecting the molecular basis of phagocyte NADPH oxidase-mediated limitation of filamentous growth *in vivo*.**

Candida albicans is a human commensal that causes life-threatening invasive infections in immunocompromised patients. Disseminated candidiasis is the 4th leading infection in hospitalized patients in the United States, and despite antifungal therapy, the mortality associated with candidemia can reach 30 to 40% (62). Innate immunity is a key mediator of resistance to disseminated infection in both mice and humans, and defects in professional innate immune cells predispose individuals to invasive candidemia (5, 26, 68).

The zebrafish larva is a unique and powerful model for noninvasively visualizing and understanding the interactions of pathogens with the innate immune system (17, 48, 56). Notably, zebrafish have similar signaling through Toll-like receptors to that in humans, express similar cytokines, and have macrophages, neutrophils, dendritic cells, mast cells, eosinophils, T cells, and B cells (78). The delayed development of T cells and B cells, which do not mature until approximately 30 days postfertilization, permits a natural focus on innate immunity in embryonic and larval infection models. A larval model of candidemia offers several advantages compared to other recently described models of zebrafish infection with *C. albicans*. Specifically, the adult zebrafish candidemia model does not permit real-time visualization of infection or morpholino (MO)-directed gene knockdown, both of which are techniques available with the larval host (19). Also, while others have described a localized embryonic zebrafish infection model (19), it is not clear if and how these infections parallel human diseases of clinical importance, such as disseminated candidiasis. A larval zebrafish model of disseminated candidiasis offers a clinically relevant disease in a transparent and small host that relies on innate immunity and can be perturbed by antisense morpholino-mediated gene knockdown (43, 48, 87). These advantages have been exploited by others to identify novel immune mediators of infectious disease (78, 79) and provide a unique opportunity to address the molecular nature of *in vivo* interactions between *C. albicans* and immune cells in the context of a live host.

One key mediator of innate immunity to *C. albicans* is the phagocyte NADPH oxidase complex, also referred to as NOX2 or the phagocyte oxidase, which is expressed in both macrophages and neutrophils and is defective in chronic granulomatous disease (6). NADPH oxidase catalyzes the production of microbicidal reactive oxygen and nitrogen species (ROS and RNS), in addition to driving changes in ion concentrations and phagosomal redox state (6, 72, 74). The NADPH oxidase is required for neutrophils to inhibit the *C. albicans* yeast-hypha switch *in vitro* (47), although its role in regulating *C. albicans* morphology *in vivo* has not been tested. Other *in vitro* experiments have linked the fungal oxidative stress response to both cellular defense against oxidative attack and inhibition of the yeast-hypha transition (1, 3, 15). However, the ultimate effect of ROS *in vivo* is unclear because it has also been reported that mild oxidative stress can enhance polarized growth in a thioredoxin-regulated manner *in vitro* (24, 59). The nature of oxidative stress *in vivo* has been explored during mouse candidemia

* Corresponding author. Mailing address: Department of Molecular and Biomedical Sciences, University of Maine, 5735 Hitchner Hall, Orono, ME 04469. Phone: (207) 581-2890. Fax: (207) 581-2801. E-mail: robert.wheeler@umit.maine.edu.

† Supplemental material for this article may be found at http://ec.asm.org/.

‡ Publication no. 3190 of the Maine Agricultural and Forest Experiment Station.

▽ Published ahead of print on 6 May 2011.

(31), but there has been no suitable model for real-time monitoring of oxidative stress *in vivo* during infection to address the dynamics of the response. A greater understanding of both the dynamics of oxidative attack and the consequences of defective phagocyte ROS and RNS production on fungal growth and morphology *in vivo* could have an impact on the treatment of immunocompetent and immunocompromised patients with disseminated fungal infections.

To image and understand host-fungus interactions in the context of a live host, we developed the zebrafish larva as a transparent vertebrate model of disseminated candidiasis. We show that this infection faithfully reproduces many aspects of candidemia in mammalian hosts, with *C. albicans* disseminating throughout the host, proliferating, and killing the host. We describe the consequences of phagocytosis of *C. albicans* in the intact host and describe how this event can lead to a temporary impasse in which neither host cells nor fungi perish immediately. We also demonstrate that the activities of fungal and host factors are conserved in this infection model, including a dependence on fungal hyphal growth for virulence and a host requirement of NADPH oxidase for resistance to infection. Finally, we exploited the power of this model to noninvasively visualize the cellular impact of the loss of NADPH oxidase activity. We found that the host NADPH oxidase is the major cause of oxidative stress in *C. albicans* during infection and is of vital importance in both limiting fungal proliferation and limiting filamentous growth.

MATERIALS AND METHODS

Zebrafish care and maintenance. All zebrafish were kept in recirculating systems (Aquatic Habitats, Apopka, FL) at the University of Maine Zebrafish Facility. Water temperature was kept at 28°C. All zebrafish care protocols and experiments were performed in accordance with NIH guidelines under Institutional Animal Care and Use Committee (IACUC) protocol A2009-11-01. Larvae were grown at a density of 50/dish in 10-cm petri dishes containing 60 ml egg water (deionized water with 60 mg/liter Instant Ocean salts [Spectrum Brands, Mentor, OH]). The fish strains used are described in Table S2 in the supplemental material. Egg water was supplemented with 0.00003% methylene blue for the first 24 h to prevent microbial growth. Larvae were cleaned by changing of the egg water daily. Zebrafish were not grown in water containing 1-phenyl-2-thiourea (PTU) to prevent pigmentation, because this was not necessary for viewing fungus-immune interactions and anecdotal evidence of our own and others (49) suggests the possibility that PTU could alter infection dynamics. All zebrafish care and husbandry procedures were performed as described previously (83).

Fungal strains and growth conditions. *Candida albicans* strains are described in Table S1 in the supplemental material. The *CTA1-GFP* strain (31) was kindly provided by Deborah Hogan (Dartmouth Medical School). *C. albicans* strains were grown on yeast-peptone-dextrose (YPD) agar (Difco; 20 g/liter peptone, 10 g/liter yeast extract, 20 g/liter glucose, 2% agar). For infections, liquid cultures of *C. albicans* were grown overnight in YPD at 37°C. Overnight cultures were washed in calcium- and magnesium-free phosphate-buffered saline (PBS; Lonza, Walkersville, MD) three times, counted on a hemocytometer, and adjusted to a concentration of 1×10^7 cells/ml.

Engineering of prototrophic yCherry-expressing *C. albicans* strains. The plasmid CIp-ADH1p-mCherry (40) was kindly provided by Neta Dean (SUNY-Stonybrook). This plasmid contains the yeast codon-optimized mCherry gene, referred to here as yCherry, under the control of the constitutive *ADH1* promoter, with the *URA3* marker. To replace the *URA3* marker with the nourseothricin resistance marker (*NAT*^{r}) in this plasmid, we amplified a PCR fragment by using primers CaURA3NAT-F and CaURA3NAT-R to amplify a sequence from pJK795 (77), including the P_{tef}-*NAT*^{r}-T_{tef} cassette and introducing long flanking regions homologous to the 5′ and 3′ ends of the *URA3* open reading frame. Plasmid CIp-ADH1p-mCherry and this PCR fragment were cotransformed into *Saccharomyces cerevisiae* strain BY4742 (12), and nourseothricin-resistant colonies were selected on YPD plus 100 μg/ml nourseothricin (Werner Bioagents, Jena, Germany). The plasmid was isolated, subjected to diagnostic PCR, digested with SalI, and transformed into *C. albicans* strains by use of lithium acetate (35, 77). Chromosomal integrants at the *ADH1* locus were selected on 100 μg/ml nourseothricin and verified by PCR, using primers P_{ADH1} and CherryRev.

MO knockdown. Modified antisense oligonucleotides (MOs) designed to knock down translation of p47^{phox} (NCF1; GenBank accession no. NM_001030071) or p91^{phox} (CYBB; GenBank accession no. NM_200414) were designed either overlapping the AUG start codon or just 5′ of the AUG codon. These had the following sequences: for p47^{phox}, CGGCGAGATGAAGTGTGTGAGCGAG; for p47$^{phox\text{-}2}$, TGTCTCACGTATGTTTCAGCCATCC; and for p91^{phox}, CAAG AGAAAGTGAGCCACAAGACAG. Morpholinos were ordered from Gene Tools (Philomath, OR) and reconstituted in nuclease-free water, and appropriate dilutions were stored in Danieau buffer [58 mM NaCl, 0.7 mM KCl, 0.4 mM $MgSO_4$, 0.6 mM $Ca(NO_3)_2$, 5.0 mM HEPES, pH 7.6]. A standard control morpholino from Gene Tools (directed to a human-specific gene) was used at the indicated doses in all experiments. MOs directed against NADPH oxidase components were injected into 1-cell embryos in 5-nl doses to achieve 2.5 or 3.5 ng of morpholino/injection as described previously (61). Morpholino sequences are detailed in Table S3 in the supplemental material. Morpholino injection stocks were prepared in 0.01% phenol red or 0.16% Alexa 547- or Alexa 647-labeled dextran (molecular weight [MW], 10,000; Invitrogen, Carlsbad, CA) for visualization of injection success. An MPPI-3 pressure injection system (Applied Scientific Instrumentation, Eugene, OR) was used for all injections. For p47^{phox} MO synergy experiments, embryos were coinjected with 1.25 ng p47^{phox} and 1.75 ng p47$^{phox\text{-}2}$.

Microinjection. Zebrafish at the prim25 stage (approximately 36 h postfertilization) were staged according to the method of Kimmel et al. (41), manually dechorionated, and anesthetized in Tris-buffered tricaine methane sulfonate (tricaine; 200 μg/ml) (Western Chemicals, Inc., Frendale, WA). For infection, 5 to 10 nl of PBS or *C. albicans* suspension at 1×10^7/ml in PBS was microinjected through the otic vesicle into the hindbrain ventricle (to achieve a dose of approximately 10 CFU).

Fluorescence microscopy. An Olympus IX-81 inverted microscope with an FV-1000 laser scanning confocal system was used for confocal imaging (Olympus). Objective lenses with powers of ×4/0.16 numerical aperture (NA), ×10/0.4 NA, ×20/0.7 NA, ×40/0.9 NA, and ×40/0.75 NA were used. Fish were anesthetized in Tris-buffered tricaine methane sulfonate (200 μg/ml) and further immobilized in a mixture of 0.5% low-melting-point agarose (Lonza, Walkersville, MD) in egg water including tricaine. Images are overlays of fluorescence image panels (red-green) or overlays of differential interference contrast (DIC) and fluorescence images. yCherry and enhanced green fluorescent protein (EGFP) fluorescence was detected by optical filters for excitation/emission at 543 nm/610 nm and 488 nm/510 nm, respectively. Images for Fig. 6C were taken with a Zeiss Axiobserver Z1 microscope equipped with a Vivatome system (Carl Zeiss Microimaging, Thornwood, NJ). All time-lapse imaging was performed using a Delta T5 heated stage (Bioptechs, Butler, PA). Larvae were maintained in 0.5% low-melting-point agarose with egg water and tricaine in cover glass-bottom culture dishes, kept at a constant temperature of 28°C, and imaged over time with an Olympus FV-1000 laser scanning confocal system. To quantify the ratio of green to red fluorescence of the WT-OXYellow strain, confocal images were analyzed with ImageJ (National Institutes of Health). Individual yeast and filament (hyphal or pseudohyphal) segments were traced using the "polygon" tool. Traced segments were then analyzed using the color histogram function with an output of average red or green intensity per pixel. The ratios for at least 50 yeast and filament (hyphal or pseudohyphal) segments were analyzed and graphed using JMP 7.0 (SAS, Cary, NC).

Enumeration of fungal burdens. Larvae infected with *C. albicans* were incubated at 28°C during infection. At each time point, 5 or 10 living larvae were anesthetized in tricaine, collected in 100 μl of egg water, and homogenized with a hand-held Kontes microgrinder (Research Products International, Inc., Mt. Prospect, IL). Four hundred to 900 μl of penicillin-streptomycin stock solution (Lonza, Walkersville, MD) was added to bring the final volume to 500 μl to 1 ml. Tenfold serial dilutions were made in penicillin-streptomycin stock solution, and 100 μl of each dilution was plated in triplicate onto YPD agar. Plates were incubated for 24 h at 37°C. Viable colonies were counted, and burdens were calculated per fish. Fungal burdens are graphed as CFU per fish. Error bars represent standard deviations. Student's *t* test was used to determine statistical significance. Three independent experiments were conducted.

Respiratory burst assay. The respiratory burst assay was performed using H_2DCF-DA (dihydrodichlorofluoresceindiacetate) as described previously (38), with a few minor changes. Four to eight larvae per treatment were induced with phorbol 12-myristate 13-acetate (PMA), and four to eight other larvae were not

induced for each treatment group (control MO or p47^{phox} or p91^{phox} MO). A Synergy2 plate reader (Biotek, Winooski, VT) was used to measure fluorescence every hour for a total of nine measurements. Excitation and emission wavelengths were 485 nm and 528 nm, respectively. Differences in the ratios (induced/uninduced) of control and p47^{phox} or p91^{phox} morphants were examined using bootstrapped confidence intervals obtained from 1,000 replicates, using the PopTools add-in for Microsoft Excel. The degree of significance was determined by observing whether 95%, 99%, and 99.9% confidence intervals overlapped.

Imaging and quantification of fungal morphology in crushed fish. To image fungal morphology without interference of melanophores and internal organs, we euthanized individual fish and placed them onto microscope slides, removed all excess water, and added a coverslip. This immediately crushed the fish into a thin aqueous layer without compromising the fungi. Crushed fish were imaged by epifluorescence microscopy on an Olympus IX-81 microscope using IP Lab (version 3.0; Scanalytics) or on a Zeiss Axiovert microscope using Axiovision (release 4.7; Carl Zeiss Microimaging, Thornwood, NJ). For each fish, fields were imaged to document all of the fungi in the entire fish. For analysis, images were overlaid in Photoshop (Adobe Inc., San Jose, CA). An illustration of the methodology is shown in Fig. S6 in the supplemental material. Regions with well-separated fungal cells were annotated by tracing filamentous (hyphal or pseudohyphal) cells (in one layer) and yeast cells (in another layer). For each annotated layer, the area was calculated by ImageJ (National Institutes of Health). For each fish, percent filamentous (hyphal or pseudohyphal) growth was calculated based on the number of countable cells. For any areas that had too dense a concentration of fungi for reliable counting, the percent filamentation for the image field was calculated and the uncountable area was divided accordingly into yeast and filamentous growth.

RESULTS

Hindbrain ventricle infection route leads to lethal disseminated candidiasis in zebrafish larvae. Several routes of infection (immersion, caudal vein, Duct of Cuvier, and hindbrain ventricle) were attempted to establish a disseminated infection in transparent zebrafish larvae. We initially attempted bath infection with up to 10^8 *C. albicans* yeast cells/ml of water. These bath infections of fish aged to 3 to 6 days postfertilization resulted in no mortality and no fungal invasion past the gastrointestinal tract. To date, our attempts at infection of the yolk have resulted in universal lethality within 24 h, while common cardinal vein infections yielded yolk-focused infections, similar to what was recently published (19). When these infected fish were examined, however, there was little to no apparent dissemination. Thus, these methods did not immediately offer a good model for disseminated candidiasis, which is the lethal form of human candidiasis. We also attempted to inject fish at 2 to 3 days postfertilization via the caudal vein, but our attempts resulted in too much lethality, even using buffered saline as a control. This was probably due to the relatively large bore needle required to inject *C. albicans* yeast (3 to 5 μm in diameter). In contrast, our initial infections of the hindbrain of prim25-stage fish embryos yielded a disseminated *Candida albicans* infection in which the fungus replicated rapidly and killed over half of the fish within the first 2 days postinfection.

Utilizing the hindbrain infection route, we found that *C. albicans* disseminated throughout the fish, and both yeast and filamentous fungi were found as far away as the tail (Fig. 1A and insets). Fish were microinjected in the hindbrain ventricle with 10 to 20 yeast cells/fish, as determined retrospectively by counting viable CFU from homogenates immediately following infection (Fig. 1B). After infection, the fungi proliferated rapidly, and by 24 h postinfection (hpi), they were at 100-fold greater numbers per surviving fish (Fig. 1B). By 48 hpi, the fungal burden in surviving fish dropped precipitously, to only five times that of the initial injection amount. The remaining live *C. albicans* and fish continued to survive for several days, although we did not examine fungal burdens beyond 6 days postinfection to determine how long the infected fish remained colonized. In parallel with fungal burden measurements, we also monitored fish for mortality. In over 20 experiments performed, we found that 49% ± 16% of infected fish succumbed to infection within 5 days postinfection, with the majority of mortality in the first 48 hpi (Fig. 1C). To determine if the mortality was pathogen specific, we also infected fish with heat-killed *C. albicans* and prototrophic *Saccharomyces cerevisiae*. Neither dead *C. albicans* nor live *S. cerevisiae* caused mortality (see Fig. S1 in the supplemental material).

It is notable that the fungal burdens shown in Fig. 1B were measured in surviving fish and do not include fish that succumbed to the infection; this methodology eliminates problems associated with assaying fungal burdens within dead fish, which disintegrate over time or permit the postmortem growth of fungi. When we looked at fungal burdens of dead fish, we found a much higher burden per fish than the value for live fish (see Fig. S2 in the supplemental material). The high fungal burden at 24 hpi shown in Fig. 1B includes both fish that died by 48 hpi and fish that cleared the infection. Examination of fungal burdens within individual fish at 24 hpi demonstrated a wide range of fungal burdens per fish. This suggests that many of the fish with high fungal burdens that were still alive at 24 hpi succumbed to the infection by 48 hpi, while fish with lower burdens likely cleared the infection.

***C. albicans* switches rapidly to hyphal growth but reverts to yeast form after immune infiltration.** To visualize the extent of filamentation during infection, we noninvasively imaged the morphological form of *C. albicans* for the first 24 hpi. We found that the infecting yeast-form cells germinated within the first 6 h, but by 24 hpi, they reverted to yeast-form growth in most of the surviving fish (Fig. 2A). To reinforce these qualitative results, we scored individual fish for the presence of hyphae and found that 70% ± 8% of fish had at least one hyphal cell at 6 hpi, but this number was sharply decreased, to 27% ± 11%, by 24 hpi (Fig. 2B). In heavily infected fish that were moribund and likely to soon succumb to infection, we often found extensive filamentation that eventually broke through the skin of the fish (see Fig. S3A and Movie S1 in the supplemental material). In many cases, we also found blocked blood vessels (see Fig. S3B and Movie S2) and tissue damage throughout the fish.

To assess if the immune response could explain the fungal switch to yeast-form growth, we visualized fungal cells and the immune response noninvasively. We used transgenic *fli1*:*EGFP* fish with EGFP-expressing macrophage-like cells and endothelium (45, 65) and *mpx*:*GFP* fish with EGFP-expressing neutrophils (66). We infected these fish with *C. albicans* expressing yCherry (a version of mCherry that is codon optimized for *Candida* spp.) and coimaged fungi and innate immune cells. We found that macrophage-like cells and neutrophils phagocytosed yeast-form *C. albicans* and wrapped themselves around filamentous fungi. Figure 2C and Movie S3 in the supplemental material show several EGFP-positive neutrophils and several EGFP-negative macrophage-like cells that have phagocytosed *C. albicans* yeast. Time-lapse visualization of phagocytosis in *fli1*:*EGFP* larvae (Fig. 2D; see

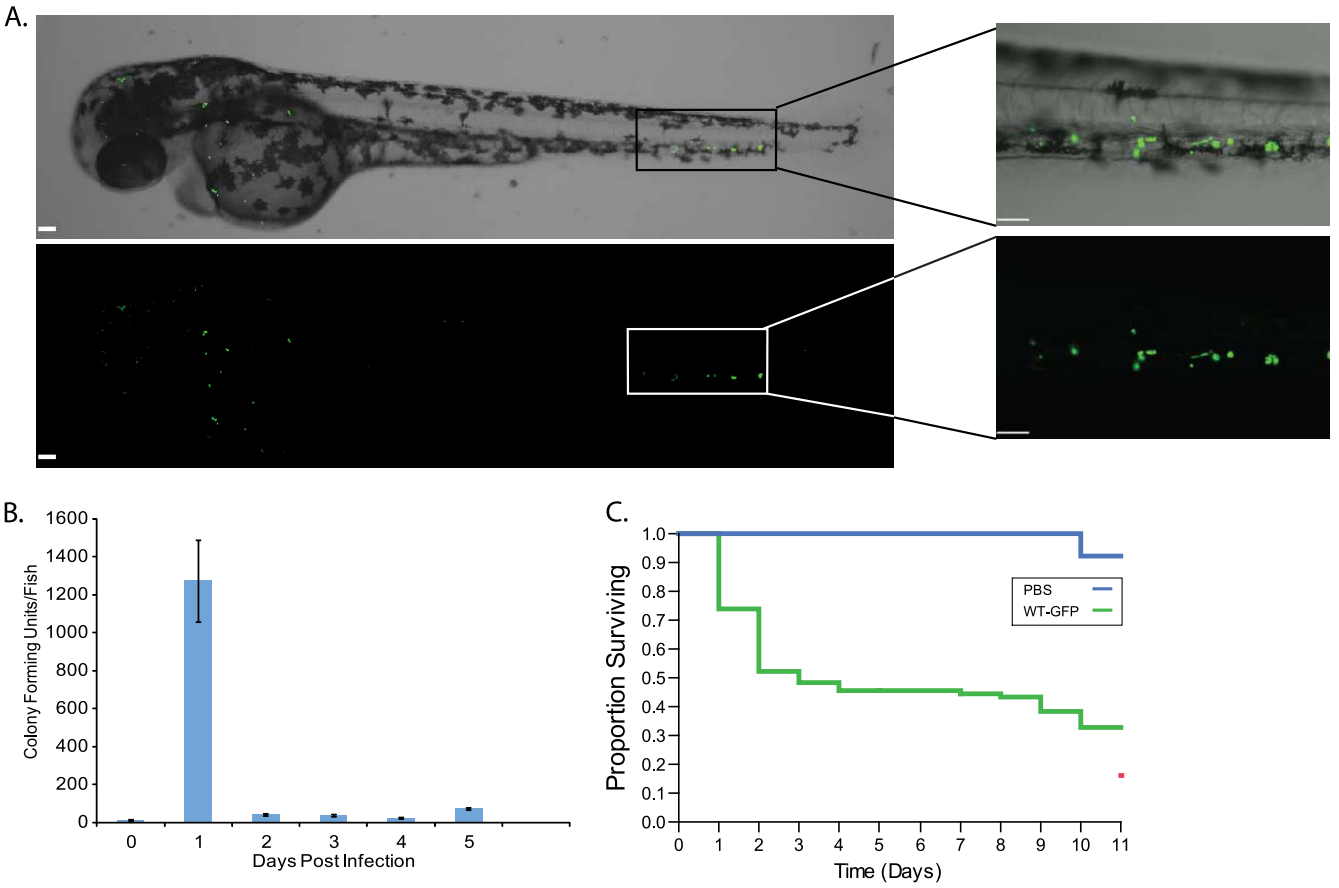

FIG. 1. Injection of *C. albicans* into zebrafish larvae causes disseminated infection and significant mortality. Wild-type GFP-expressing (WT-GFP) *C. albicans* cells (11 ± 4 CFU, as measured in homogenates at 0 hpi) were injected into the hindbrain ventricle of wild-type AB larvae at the prim25 stage. The results in each panel are representative of at least three independent experiments. (A) Confocal imaging of disseminated infection at 24 hpi. Bars, 100 μm in large images and 50 μm in insets. (B) Fungal burdens determined by serial dilution and growth on YPD plates. Error bars represent standard deviations. (C) Kaplan-Meier survival curve from a representative experiment. WT-GFP strain-infected fish had significantly more mortality than PBS-injected controls ($P < 0.0001$ by log rank test).

Movie S4) also shows apparent chemotaxis of a phagocyte toward extracellular fungi.

The dynamics of immune infiltration and changes in fungal morphology are consistent with the idea that immune activity plays an important role in controlling both fungal proliferation and morphogenesis. However, it is notable that the immune system was not able to control proliferation and morphogenesis in all infected fish, such that by 1 day postinfection, the larvae were either moribund with extensive fungal hyphae or relatively healthy with a majority of yeast-form cells. We asked if the ability to control filamentous growth in the first 24 hpi is predictive of overall survival by imaging infected fish at 24 hpi and following their survival until 48 hpi. We found that fish that had restrained filamentous growth by 24 hpi (yeast-only group) all survived to 48 hpi, whereas fish with filamentous fungi (yeast and filament group) suffered significantly higher mortality between 24 hpi and 48 hpi (0% ± 0% versus 63% ± 15%; $P = 0.002$) (see Fig. S4 in the supplemental material). This suggests that the ability to control fungal morphogenesis within the first 24 hpi allows fish to survive disseminated infection.

Fate of *C. albicans* within phagocytes. After establishing that macrophage-like cells and neutrophils both engulf *C. albicans* during infection, we asked how the fungi fare inside phagocytes. *In vitro*, in the absence of most natural soluble and membrane-bound modulators of macrophages and neutrophil activity, *C. albicans* germinates inside macrophages but not inside neutrophils (16, 42, 71). The presence of these cues *in vivo* may lead to different phagocyte activity in the intact host, as macrophage and neutrophil activity *in vitro* can be enhanced by extracellular matrix contacts and by the presence of cytokines (16, 76). In fact, using our *in vivo* model, we found two distinct patterns of phagocyte interaction with *C. albicans* in the first several hpi that differ from what has been described *in vitro*. Neutrophils (EGFP positive in *mpx*:*GFP* transgenic fish and containing cytoplasmic granules) phagocytosed a limited number of *C. albicans* yeast cells (between 1 and 3) and remained highly motile postphagocytosis (Fig. 2C, E, and F and Table 1). On the other hand, macrophage-like cells (EGFP positive in *fli1*:*EGFP* transgenic fish, EGFP negative in *mpx*:*GFP* transgenic fish, and lacking cytoplasmic granules) phagocytosed more *C. albicans* yeast cells (up to 9) and had greatly

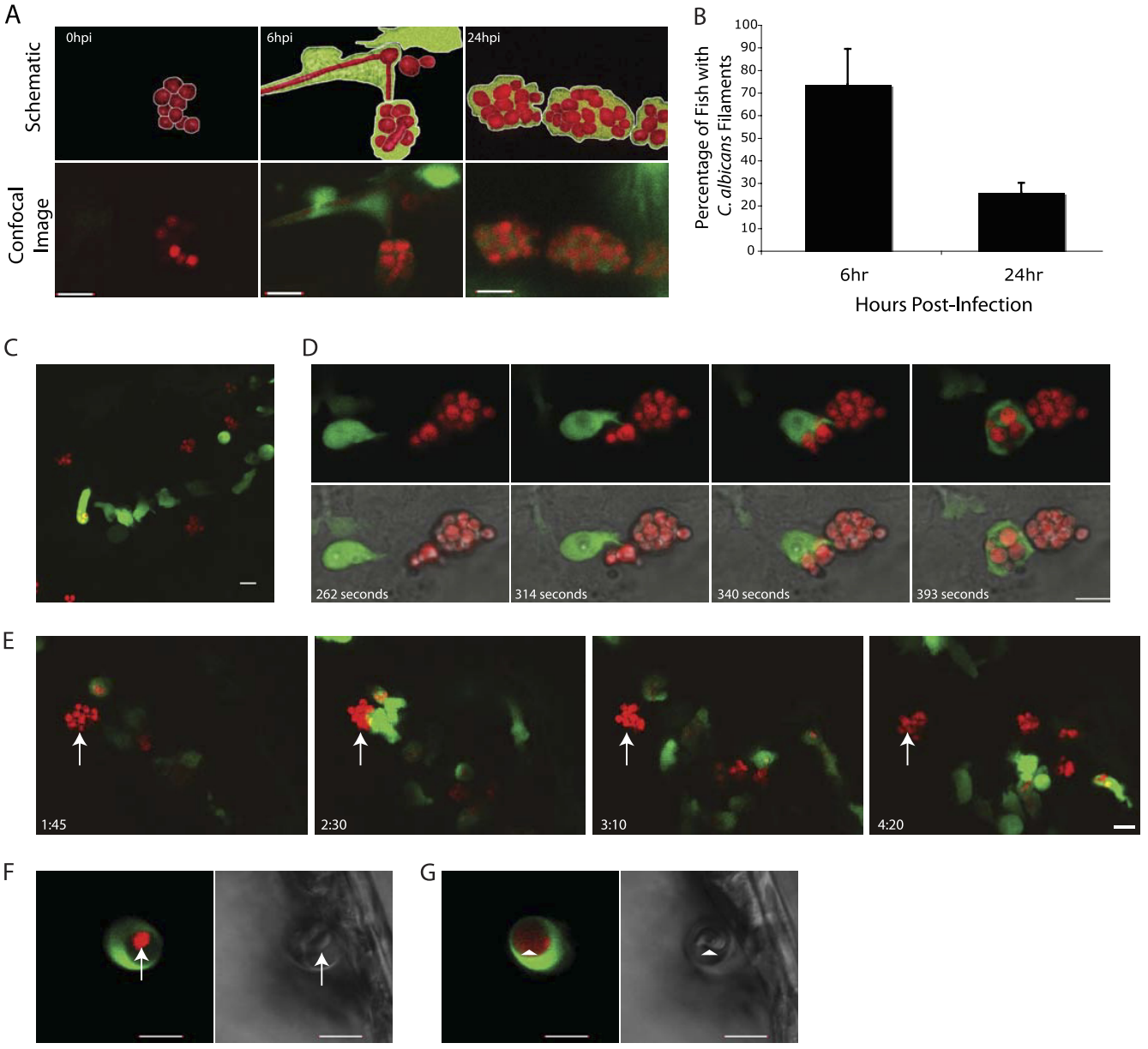

FIG. 2. Noninvasive imaging of innate immunity-fungus interactions. For all panels, prim25-stage embryos were infected with 10 to 15 CFU of CAF2-yCherry in the hindbrain ventricle. Bars = 10 μm. (A) Infected *fli1*:*EGFP* larvae with green macrophages were imaged at 0, 6, and 24 hpi by confocal microscopy. Images at 0 and 6 hpi are individual optical sections, and images at 24 hpi are *z*-stack projections of 15 optical slices. (B) Percentages of filaments in wild-type AB control morphants. Data shown are the averages and standard deviations for three independent experiments. (C) An infected *mpx*:*GFP* embryo was imaged from 0.25 to 4.5 hpi by confocal microscopy. Shown is a *z*-stack projection of 30 optical slices from 4 hpi. A movie of the three-dimensional reconstruction of these slices is viewable as Movie S3 in the supplemental material. (D) An infected *fli1*:*EGFP* larva was imaged from 2 to 2.2 hpi by confocal microscopy. Individual optical sections are shown. The entire image series is viewable as Movie S4. (E) An infected *mpx*:*GFP* larva was imaged from 0.25 to 4.5 hpi by confocal microscopy. The EGFP-negative macrophage followed in the time-lapse series is indicated with a white arrow. The figure panels are *z*-stack projections of 19 to 30 optical slices covering the entire *z* space of the hindbrain ventricle. The entire time-lapse series is viewable as Movie S5. (F and G) An infected *mpx*:*GFP* larva was imaged at 5 hpi by confocal microscopy. Shown are single optical slices from a *z* series encompassing a single EGFP-positive neutrophil with two fungi inside. The entire *z* series is viewable as Movie S6. (F) Phagosome with live fungus. yCherry is concentrated within the fungal cytoplasm and limited to the fungal cell. Arrows indicate the position of intact fungus. (G) Phagosome with killed fungus. yCherry is no longer concentrated and limited to the fungal cytoplasm and has dispersed throughout the phagosome. Arrowheads indicate the remaining cell wall.

reduced motility postphagocytosis (Fig. 2A and D and Table 2). We refer to these macrophage-like cells as macrophages, because they exhibit overall characteristics most similar to what has been described for macrophages (49) and dissimilar to those described for neutrophils, the other major phagocytic cells present at this time of development (46).

We found that phagocytosis can lead to an impasse inside macrophages in which a macrophage inhibits germination of

TABLE 1. Fate of *C. albicans* within neutrophils[a]

Expt no.[b]	No. of PMN without fungi inside	No. of PMN with fungi inside	Mean no. of fungi per PMN	Total no. of fungal cells	No. of killed fungi[c]
1	17	20	1.6	32	0
8	32	8	2.25	18	1
9	38	10	1.7	17	1

[a] There were no germinating fungi observed during the time course in any experiment. PMN, polymorphonuclear leukocytes.
[b] All experiments were done with zebrafish with the *mpx*:*GFP* genotype.
[c] Killed fungi were fungi for which no red fluorescence was associated with the fungus but red fluorescence filled the phagosome.

TABLE 2. Fate of *C. albicans* within macrophages[g]

Expt no.	No. of macrophages[d]	Mean time (h) of visualization	Mean no. of fungi per macrophage[e]	Total no. of fungal cells	No. of germinating fungi[f]
1[a]	4	2.25	4.5	18	0
2[b]	2	5	4.5	9	1
3[c]	10	4.9	3.7	37	0
4[c]	34	3.5	5.1	173	0
5[b]	16	2.1	3.5	56	0
6[b]	4	2.8	4.25	17	0
7[b]	7	3.6	2	14	0

[a] The host zebrafish genotype was *fli1*:*EGFP*.
[b] The host zebrafish genotype was *mpx*:*GFP*.
[c] The host zebrafish genotype was wild-type AB.
[d] Macrophages were identified on the basis of a lack of granularity, expression of EGFP in *fli1*:*EGFP* larvae, lack of EGFP expression in *mpx*:*GFP* larvae, and limited motility postphagocytosis.
[e] Measured for macrophages with one or more internalized fungi.
[f] Number of observed events during the time course.
[g] Dividing fungi were observed in experiments 1 and 5. In experiment 1, two yeast cells within one macrophage divided to make four cells, for a total of nine yeast cells in the macrophage by the end of the time course. In experiment 5, two yeast cells within two different macrophages divided, for a total of four yeast cells in one macrophage and six yeast cells in the other by the end of the time course.

C. albicans but does not kill the fungus. This situation can last for at least 4 h (Fig. 2E; see Movie S5 in the supplemental material). In this particular case, there were more fungi in the macrophage at the end of the time-lapse experiment (10 versus 8), even though there were no further phagocytic events. Increases in the number of yeast cells in a macrophage, in the absence of additional phagocytosis, were observed in two other cases (Table 2). These data suggest that fungi not only remain viable but are able to divide within macrophages. In a total of seven time-lapse experiments, we visualized 77 macrophages with ingested yeast cells. Contrary to our expectations based on *in vitro* reports, we witnessed germination of only one yeast cell within a macrophage (among a total of 324 yeast cells followed for an average of 3.5 h) and did not observe a single event in which the fungus germinated and burst the phagocyte. By following fungal cytoplasmic yCherry fluorescence as an indicator of fungal viability, as described previously (84), we found no killing of *C. albicans* within macrophages. We did observe macrophages with filamentous fungi within them, which may be due to phagocytosis of small hyphae, as described previously (27).

Neutrophils were difficult to monitor over longer periods due to their rapid motility. To obtain a snapshot of fungal fate within neutrophils, we scored three-dimensionally reconstructed image stacks of $EGFP^+$ neutrophils in *mpx*:*GFP* larvae at 3 to 6 hpi (Fig. 2C; see Movie S3 in the supplemental material). Among 87 neutrophils and 67 phagocytosed fungi observed in 3 independent experiments, we witnessed two cases of a fungus losing membrane integrity and being destroyed (as assessed by release of cytoplasmic yCherry fluorescence). In both cases, we observed red fluorescence, which is confined to the fungal cytoplasm in intact fungi (Fig. 2F), throughout the phagosome (Fig. 2G; see Movie S6). In each case, the phagosomal red fluorescence persisted within the phagosome for over 1 h. This suggests that when a neutrophil damages a *C. albicans* cell, some cellular contents (including yCherry fluorescent protein) can be released into and persist within the phagosome for an extended period. The rarity of these events, coupled with the length of time that the dissipated yCherry protein remained visible, argues that fungi are not always rapidly killed by neutrophils *in vivo*. Neutrophils roamed in and out of the site of infection, and many did not phagocytose fungi (Table 1). These empty innate immune cells may play an indirect role in inhibiting fungal growth or may act as a backup system in case fungi escape from within phagocytes. We saw no cases of filamentous fungi within neutrophils, although we did observe neutrophils wrapping themselves around *C. albicans* filaments.

In sum, we found 2/67 fungi killed within neutrophils but 0/324 fungi killed within macrophages, suggesting that neutrophils may have a greater capacity to kill *C. albicans* than that of macrophages in the intact host. The rarity of killing events observed within neutrophils does not exclude the possibility that a larger proportion of fungi phagocytosed by neutrophils may eventually have been killed at a time after our imaging, because we were unable to follow individual interactions over time. Yet these *in vivo* time-lapse and time course data reveal the prevalence of a previously unappreciated outcome of *C. albicans*-host interaction: an impasse between fungus and phagocyte.

Yeast-hypha switch factors regulate virulence in larval zebrafish candidemia. To establish if similar genetic mechanisms regulate fungal virulence in this model and other infection models, we tested the virulence of the *efg1*Δ/Δ *cph1*Δ/Δ mutant, a hypofilamentous strain of *C. albicans* with reduced virulence in the mouse, fly, nematode, adult zebrafish, and moth models of infection (14, 18, 19, 52, 64). We found that the *efg1*Δ/Δ *cph1*Δ/Δ mutant had a reduced capacity to replicate within and kill zebrafish larvae. The hypofilamentous fungi had significantly reduced virulence ($P < 0.0001$) (Fig. 3A). In addition, infections with mutant fungi resulted in a reduced fungal burden ($P < 0.001$) (Fig. 3B). The *efg1*Δ/Δ *cph1*Δ/Δ mutant retained its ability to grow in a filamentous form as pseudohyphae (Fig. 3C), as reported previously for oral and disseminated mammalian infections (8, 67). Although the transcription factors encoded by these genes regulate a number of genes (32), these data provide a further indication that hyphal growth, seen early during infection and in larvae that succumbed to infection, plays an important role in virulence in zebrafish larval candidemia. This reinforces the parallels between disseminated infections in zebrafish and mice.

Phagocyte NADPH oxidase is required for resistance in larval zebrafish candidemia. In humans and mice, phagocyte

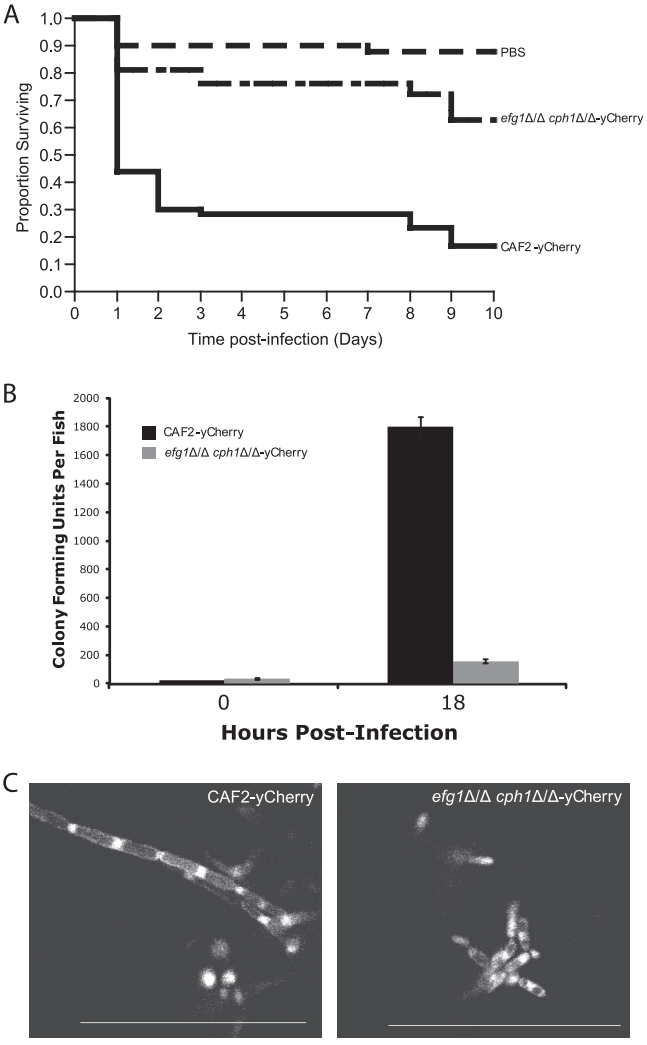

FIG. 3. Hyphal morphogenesis is required for virulence. Wild-type AB fish at the prim25 stage were infected in the hindbrain ventricle with 20 CFU of CAF2-yCherry or 35 CFU of *efg1*Δ/Δ *cph1*Δ/Δ-yCherry *C. albicans*. (A) A hypofilamentous mutant is less virulent. Wild-type CAF2-yCherry (red) or the filamentation-defective *efg1*Δ/Δ *cph1*Δ/Δ-yCherry strain (green) was used to infect 100 prim25-stage fish. The difference in survival is significant ($P < 0.0001$ by log rank test). (B) Fungal burdens are reduced in hypofilamentous *efg1*Δ/Δ *cph1*Δ/Δ-yCherry strain-infected larvae compared to those in CAF2-yCherry-infected larvae ($P < 0.001$ by Student's *t* test). Note that at 0 hpi, the infection dose was established, and for this experiment, there was a higher dose for the *efg1*Δ/Δ *cph1*Δ/Δ-yCherry strain (35 ± 6) than for CAF2-yCherry (20 ± 0). Error bars represent standard deviations for triplicate measurements. (C) Confocal imaging of infected fish at 18 hpi reveals reduced but not absent filamentation in *efg1*Δ/Δ *cph1*Δ/Δ-yCherry strain-infected larvae (right) in comparison to CAF2-yCherry-infected larvae (left). Despite growing as filaments, the *efg1*Δ/Δ *cph1*Δ/Δ-yCherry strain grows only as pseudohyphae. Bars = 50 μm. Results for all three panels were derived from the same experiment and are representative of at least three independent experiments in which doses were comparable and the dose of the *efg1*Δ/Δ *cph1*Δ/Δ-yCherry strain was greater than or equal to the dose of CAF2-yCherry.

NADPH oxidase is required for resistance to bacterial and fungal bloodstream infections (7). To test whether this mechanism is important in resistance to infection in the larval zebrafish model of candidemia, we reduced NADPH oxidase function by antisense morpholino-mediated gene knockdown. We found that knockdown of the p47^{phox} subunit of the NADPH oxidase led to a dampening of the overall respiratory burst and to greater susceptibility to infection. To measure the respiratory burst, whole live fish were stimulated with phorbol ester in the presence of dihydrodichlorofluoresceindiacetate (38). Injection of 2.5 ng of p47^{phox} morpholino caused significant dampening of the phorbol ester-stimulated respiratory burst compared to that with 2.5 ng of control morpholino ($P < 0.0001$) (Fig. 4A). To demonstrate the specificity of knockdown, we also used a second, nonoverlapping morpholino (p47$^{phox\text{-}2}$) and found synergy between the two morpholinos (see Fig. S5 in the supplemental material), suggesting that respiratory burst dampening was specific and not due to general morpholino-associated artifacts or off-target effects (29). Similar dampening was also found upon morpholino knockdown of the p91^{phox} subunit (see Fig. S5). Larvae with p47^{phox} activity knocked down (p47^{phox} morphants) had significantly greater susceptibility to infection than control morphants ($P \leq 0.01$) (Fig. 4B). The p47^{phox} morphants also had greater fungal burdens at 12, 18, and 24 hpi ($P = 0.05$, $P = 0.002$, and $P = 0.004$, respectively), although at 48 hpi, both control and p47^{phox} morphants that were alive at this point had cleared nearly all fungi (Fig. 4C and data not shown). This suggests that fish that survive the first 2 days of infection have a low fungal burden and tend to survive for the remainder of the experiment, having successfully controlled the infection. These data are consistent with reports that have shown a role of phagocyte NADPH oxidase in resistance to candidemia in both mice and humans, providing further evidence that findings with this model host will translate well to mammalian infection.

Phagocyte NADPH oxidase is required to limit *C. albicans* filamentation in larval zebrafish candidemia. We did not visualize any events in which fungi burst through phagocytes and saw very few in which fungi were killed (lost cytoplasmic fluorescence) within phagocytes (Tables 1 and 2). The inability of fungi to kill immune cells could result from a failure of the fungi to germinate at the reduced temperature of 28°C or could be due to immune regulation of fungal growth. To understand if the phagocyte NADPH oxidase plays a role in maintaining this impasse between macrophages and yeast, we imaged yCherry-expressing fungi within control and p47^{phox} morphant fish. We found that between 6 and 24 hpi, filamentation increased in p47^{phox} morphants but decreased in control morphants (Fig. 5A). To quantify this, we completely imaged individual fish at a high resolution by confocal microscopy and scored the number of *C. albicans* filaments per fish. Using this measure to compare control and p47^{phox} morphants, there was no significant difference in the percentages of fish with filamentous fungi inside at 6 hpi (70% ± 14% versus 81% ± 8%, respectively; $P = 0.32$), but there was a significantly greater percentage of p47^{phox} morphants with filamentous fungi inside at 24 hpi (27% ± 11% versus 92% ± 3%, respectively; $P < 0.001$). To examine this more closely and to eliminate potential artifacts due to pigment cells or tissue depth, we crushed fish between slide and coverslip, imaged fungal cells, and quantified the percentage of fungal growth in filamentous form (as described in Materials and Methods and illustrated in Fig. S6 in the supplemental material). When the ratio of filaments to yeast cells was quantified at 24 hpi, we found a significantly

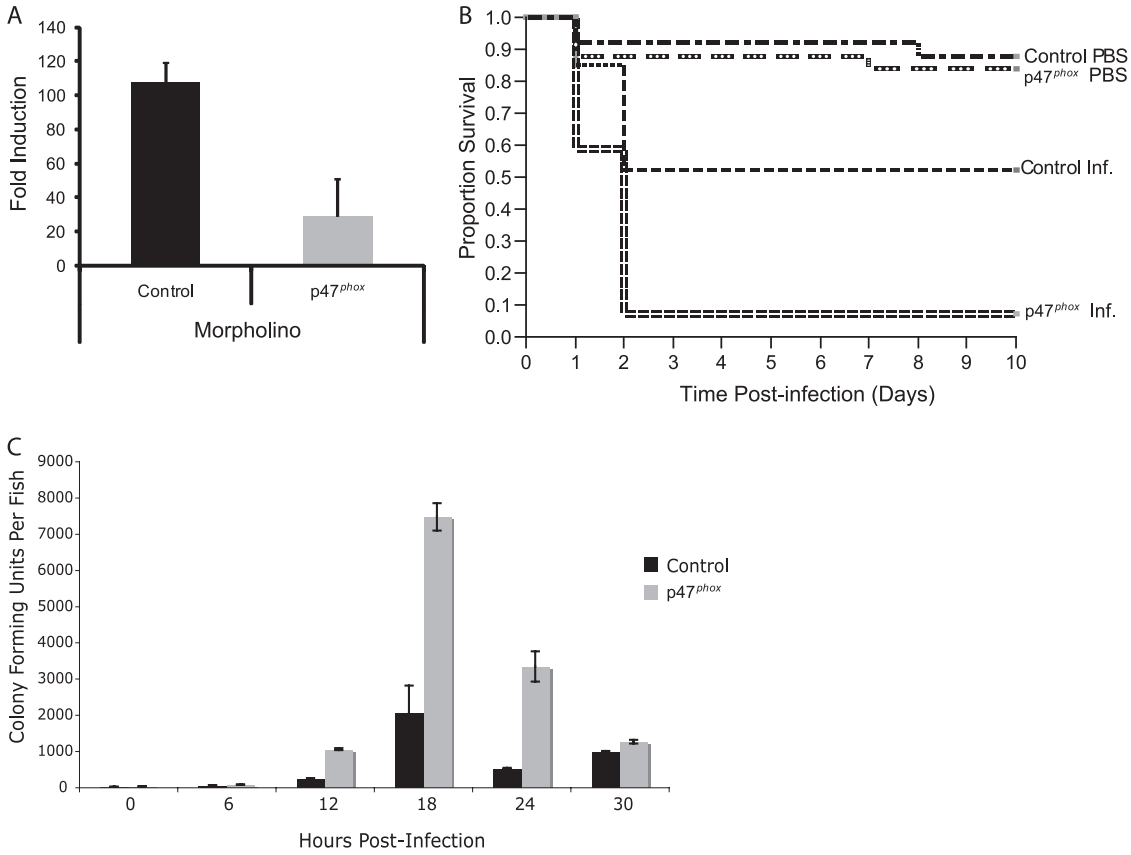

FIG. 4. Respiratory burst is required for resistance to infection. Fertilized 1-cell eggs were injected with 2.5 nanograms of control or p47^{phox} morpholino. (A) p47^{phox} morphants have a dampened respiratory burst compared to control morphants. At 48 h postfertilization, p47^{phox} or control morphants were assayed for respiratory burst activity by PMA stimulation in the presence of H_2DCF-DA. Monte Carlo analysis with 1,000 replicates was used to find the average ratio of fluorescence from 12 induced versus 12 uninduced fish, and this difference was significant ($P < 0.001$). Results are representative of three independent experiments. Error bars represent 95% confidence intervals. (B and C) One hundred morphants were infected at the prim25 stage with approximately 20 CFU of CAF2-yCherry *C. albicans*. (B) p47^{phox} morphants had reduced survival compared to control morphants ($n = 100$ for each group; $P = 0.003$ by log rank test). Note that there were significant differences ($P \leq 0.01$; Kaplan-Meier and log rank tests) between PBS- and CAF2-yCherry-injected larvae (both control and p47^{phox} morphants) but no difference ($P = 0.68$) between PBS-injected control and p47^{phox} morphants. The survival curves represent pooled data from three independent experiments with similar results. (C) p47^{phox} morphants had significantly increased fungal burdens at 12 hpi ($P = 0.05$), 18 hpi ($P = 0.002$), and 24 hpi ($P = 0.004$), as measured by Student's t test. Each bar in panel C shows the average and standard deviation of measurements from three independent experiments. Note that the average and standard deviation of the infectious dose in these three experiments, as measured at 0 hpi, was 17 ± 5 CFU for controls and 21 ± 6 CFU for p47^{phox} morphants.

higher percentage of filamentous growth in p47^{phox} morphants ($P = 0.005$) (Fig. 5B). Thus, in the absence of NADPH oxidase activity, there is significantly increased hyphal growth that accompanies greater mortality.

Phagocyte NADPH oxidase is required to generate oxidative stress *in vivo*. Based on the important role played by the phagocyte NADPH oxidase in immunity and the overall importance of oxidative stress in infection (21), it could be predicted that *C. albicans* would be subjected to oxidative stress during infection. However, it is not known when or where phagocyte NADPH oxidase-dependent oxidative stress is felt during infection. To visualize the spatiotemporal dynamics of oxidative stress in *C. albicans* during infection, we engineered a dual reporter strain we called WT-OXYellow (Fig. 6A). This strain has constitutive expression of yCherry (from the *ADH1* promoter) and oxidative stress-inducible expression of EGFP (from the *CTA1* promoter). WT-OXYellow was created by integrating the P_{ADH1}-yCherry construct into the *ADH1* locus of a *CTA1-GFP* strain recently created and characterized by the Brown laboratory (31). Upon infection of control morphants, there was little promoter activity at 6 hpi, but the oxidative stress response increased dramatically by 24 hpi (Fig. 6B, top four panels). We found widespread activation of EGFP expression in many tissues (including brain, skin, muscle, and heart), but we were not able to examine EGFP expression in blood because there were few fungi in the blood and they were moving too fast for high-resolution imaging. Because both EGFP and yCherry are cytoplasmic, the ratio of red to green fluorescence in micrographs should reflect the relative induction of the oxidative stress response. Quantitation of pixel values along lines bisecting two yeast-form cells demonstrated that red and green fluorescence did colocalize in the fungal cytoplasm in control morphants (Fig. 6C, top two panels). Stress-induced promoter activity was variable from cell to cell, as assessed by visual inspection (Fig. 6B) and by quantification of the ratio of green to red fluorescence within individual cells

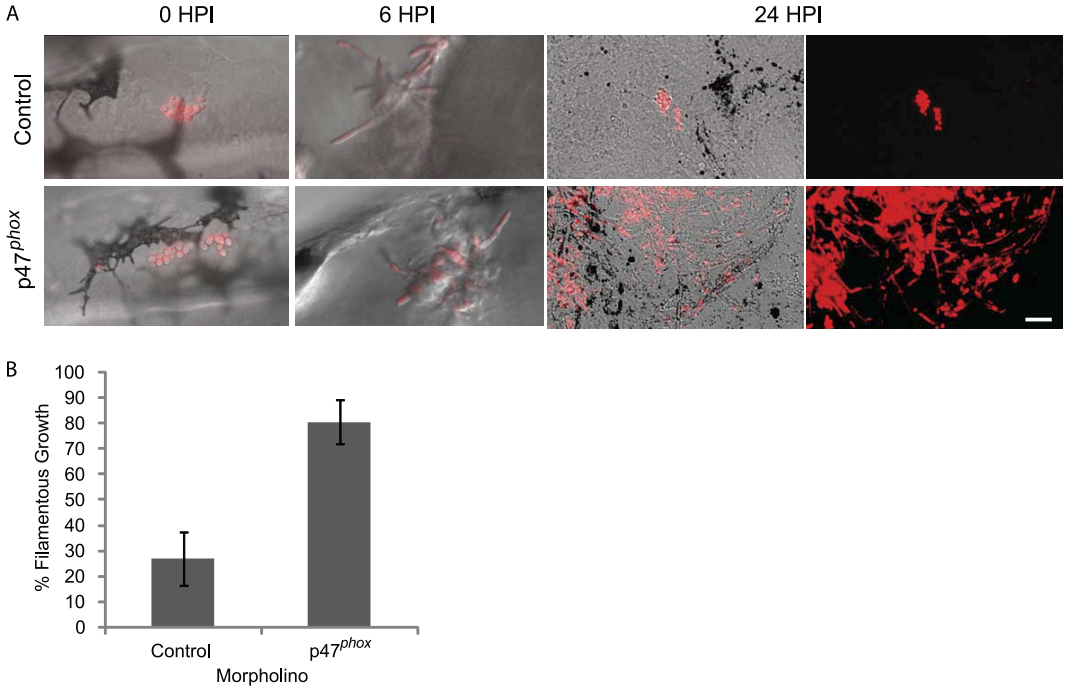

FIG. 5. Knockdown of the p47^{phox} subunit of the phagocyte NADPH oxidase enhances fungal filamentation and pathogenesis. (A) Control and p47^{phox} morphants were infected with CAF2-yCherry *C. albicans* and imaged at 0, 6, and 24 hpi. At 0 hpi, larvae were injected with approximately 20 yeast cells in the hindbrain ventricle. By 6 hpi, *C. albicans* germinated within control and p47^{phox} morphants. At 24 hpi, control morphants had only yeast-form fungi present, while p47^{phox} morphants had large chains and branches of filaments. Bar = 10 μm. (B) p47^{phox} morphants had a larger number of fungi in filamentous form than did controls at 24 hpi. Individual fish were crushed with glass coverslips onto slides and then imaged, and images were quantified for presence of yeast or filaments as described in Materials and Methods and illustrated in Fig. S6 in the supplemental material. Three independent experiments were performed (n = 11 controls and 15 p47^{phox} morphants), and data were pooled for analysis. There was a significantly higher level of filamentous growth in p47^{phox} morphants (P = 0.005 by nonparametric Wilcoxon/Kruskal-Wallis test).

(Fig. 6D). Strikingly, when p47^{phox} morphants were infected with WT-OXYellow, there was almost no detectable activity from the oxidative stress-inducible *CTA1* promoter. This was the case when we examined images (Fig. 6B, lower four panels), quantified the data in lines pixel by pixel (Fig. 6C, lower two panels), and quantified the ratio of average green fluorescence to average red fluorescence on a cell-by-cell basis (Fig. 6D). The strong induction of phagocyte NADPH oxidase-dependent oxidative stress between 6 hpi and 24 hpi is consistent with the idea that this immune mechanism contributes to the NADPH oxidase-dependent reduction in fungal filaments seen over the same period (Fig. 5).

DISCUSSION

We have exploited unique advantages of a new transparent *Candida*-zebrafish infection model to provide the first noninvasive, real-time tracking of *Candida*-immune interaction in a vertebrate host. Our results suggest that *in vivo* interactions between innate immune cells and *C. albicans* are more complex than *in vitro* observations would lead one to believe. For the first time, we were able to visualize the cellular impact of loss of host phagocyte NADPH oxidase activity on both host and pathogen, finding that it is the primary cause of oxidative stress in fungi and that it limits filamentous growth. The accessibility of this new model of candidemia promises to provide further insight into the effects of host and pathogen manipulation on the innate immune response and virulence.

The novel and uniquely positioned vertebrate model of candidemia we describe shares important characteristics of mouse candidemia yet has distinct advantages compared to previously described models of candidiasis in zebrafish. On the pathogen side, in both zebrafish and mice *C. albicans* disseminates throughout the host, causes lethality, grows as both yeast cells and hyphae, and requires Efg1p, a master regulator of the yeast-hypha transition, for full virulence (51, 52, 70). On the host side, the zebrafish and mammalian immune responses involve both macrophages and neutrophils, and immunity to the infection is strongly dependent on the phagocyte NADPH oxidase (4–6, 16, 26, 76). The larval model we describe has greater versatility than a recently reported adult zebrafish model (19), in which it is not possible to either perturb gene function with morpholinos or image the infection noninvasively by confocal microscopy. In addition, our larval zebrafish model of disseminated candidiasis, in contrast to the localized larval infections described previously (19), allows a direct comparison to disseminated disease in mammals, which is clinically the most lethal form of the disease.

The zebrafish larval model derives advantages compared to mammalian systems from its small size and transparency, permitting high-throughput screens, chemical genetic screens, and noninvasive whole-animal visualization of host-pathogen inter-

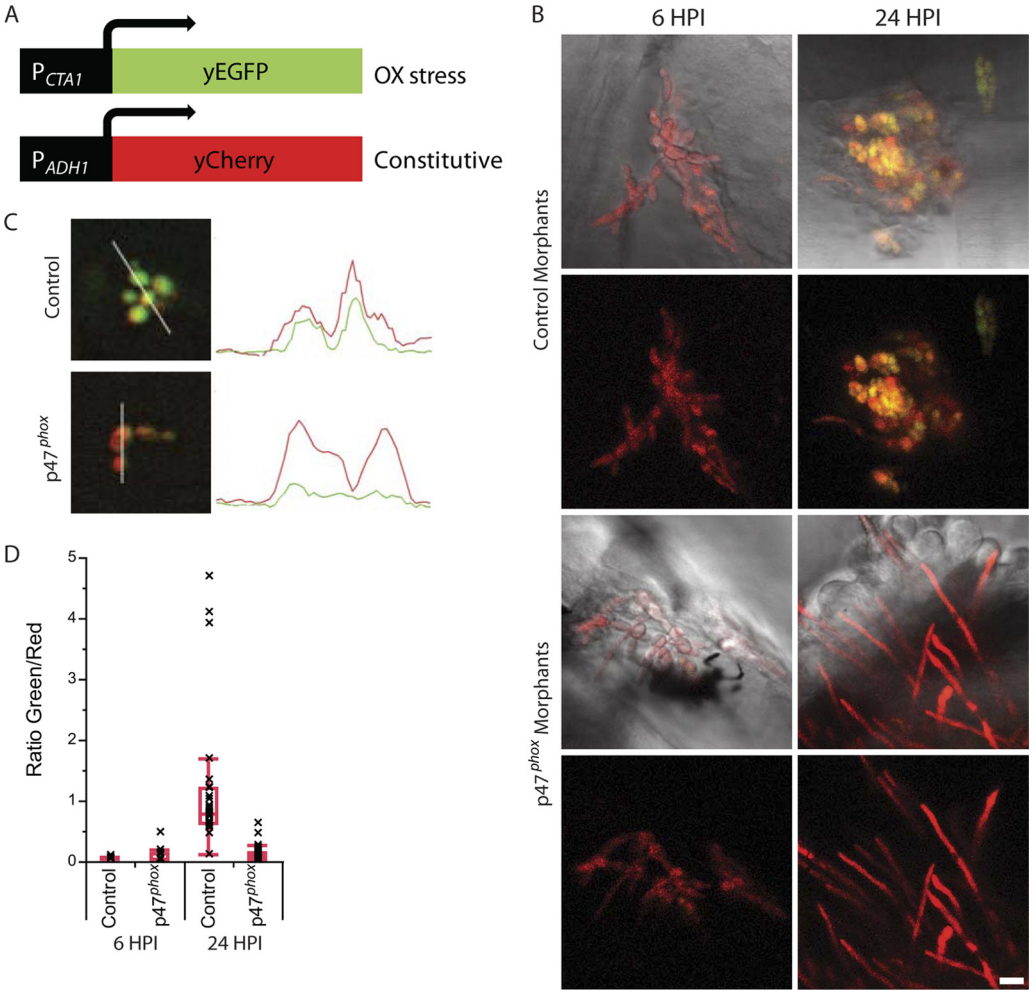

FIG. 6. *C. albicans* is subject to NADPH oxidase-dependent oxidative stress *in vivo*. (A) Schematic of dual-fluorescence oxidative stress reporter WT-OXYellow. *C. albicans* expressing EGFP from the *CTA1* promoter was transformed with the P_{ADH1}-yCherry plasmid to drive constitutive expression of yCherry. For panels B to D, one-cell fertilized eggs were injected with 2.5 ng of control or $p47^{phox}$ morpholino and infected with 10 to 15 CFU of WT-OXYellow at the prim25 stage. (B) Fungi infecting $p47^{phox}$ morphants exhibit little to no EGFP fluorescence, indicating no oxidative stress to the *Candida*. Infected control and $p47^{phox}$ morphants were imaged by confocal microscopy at 6 and 24 hpi. Bar = 10 μm. (C) Infected control and $p47^{phox}$ morphants were imaged by Vivatome microscopy, and line histograms of red and green fluorescence were compared. Yeast cells within controls (top) had correlated green and red fluorescence, indicative of cytoplasmic fluorescence. In contrast, yeast cells within $p47^{phox}$ morphants (bottom) displayed only red fluorescence and no corresponding green fluorescence. (D) Quantitation of confocal images of individual yeast cells and filament segments taken at 24 hpi was performed using ImageJ software to determine the average fluorescence per pixel as described in Materials and Methods. There was a significantly higher average green/red ratio at 24 hpi for control morphants than that for $p47^{phox}$ morphants ($P < 0.0001$; Student's *t* test) and that for controls at 6 hpi ($P < 0.0001$; Student's *t* test). Box plot whiskers represent the 1.5 interquartile range either below or above the lower or upper quartile, respectively. The results are representative of two independent experiments.

action (2, 48, 56, 78, 79). Invertebrate models of candidiasis have similar advantages but lack specialized cells analogous to vertebrate immune cells (e.g., macrophages, neutrophils, dendritic cells, eosinophils, basophils, T cells, and B cells). Furthermore, in contrast to our zebrafish host, *Drosophila* and *Caenorhabditis* become permissive hosts for *C. albicans* infection only when genetic mutants with compromised immune systems are utilized (18, 34). Notably, anatomical and immune similarities among vertebrates have empowered translation of findings from zebrafish into progress on human disease (11, 17, 39, 54, 79, 82).

Exploiting the transparency of the zebrafish larva, we noninvasively imaged *C. albicans* inside macrophages and neutrophils and found that phagocytosis can result in a standoff wherein fungi survive and divide but neither germinate nor lyse the host cell. This temporary impasse is not typically seen *in vitro*, where phagocytosed *C. albicans* rapidly germinates within and lyses macrophages or, conversely, is rapidly destroyed by neutrophils (16, 33, 42, 53, 71). Our relatively short-term observations (on the order of hours) do not yet answer whether the impasse results in a type of long-term intracellular proliferation like that observed for *Mycobacterium marinum*, which would be a novel virulence strategy for *C. albicans*. The apparently enhanced ability of macrophages to block germination may be due to soluble factors and extracellular matrix attachments that are present *in vivo* but not *in vitro* (9, 16, 44,

60). There could be host-specific factors, such as intrinsically greater activity of macrophages or reduced germinative capacity of *C. albicans*, within zebrafish. However, zebrafish and mammalian macrophages are functionally comparable (17, 48, 49, 56, 78), and the uncontrolled filamentation observed in p47^{phox} morphants argues against an inherently impaired capacity for germination. The presence of live *C. albicans* persisting in phagocytes suggests the intriguing possibility that like other fungi, bacteria, and viruses, *C. albicans* may use phagocytes to disseminate within the host (20, 28, 48, 86).

This is the first study to track cellular host responses to fungal infection within the host over time, quantifying the number of fungi per immune cell, fungal division, and fungal death during the early hours of infection. Although the larval zebrafish model has been exploited to qualitatively describe immune cell migration and behavior in infection (13, 22, 25, 37, 46, 50, 57, 80, 81), ours is one of only a few studies to quantify host-pathogen interaction events (23, 79). Our findings of more phagocytosis exhibited by macrophages than by neutrophils are similar to what has been described qualitatively for phagocytosis of *Listeria* spp. (50), *Escherichia coli* (46), *Staphylococcus aureus* (63), *Burkholderia* spp. (81), and *Pseudomonas aeruginosa* (13). Only one other report has quantified phagocytosis by zebrafish macrophages and neutrophils *in vivo* (23), and similar to our data, that study found that macrophages phagocytosed more mycobacteria than neutrophils did. Thus, larval zebrafish macrophages apparently have a greater phagocytic role than neutrophils for Gram-negative, Gram-positive, acid-fast, and fungal pathogens. However, the overall role of macrophages in immunity to *C. albicans* remains to be tested. Fortunately, two recently described transgenic fish lines (30, 36) should permit the specific ablation of macrophages to ask this previously inaccessible question.

Our data provide the first *in vivo* evidence in any infection model that the phagocyte NADPH oxidase regulates filamentation of *C. albicans* within the intact host. This is consistent with *in vitro* observations that neutrophils and macrophages lacking NADPH oxidase activity have a reduced ability to kill *C. albicans* and fail to inhibit germination (33, 47). Neutrophils exhibit filament-biased killing and growth inhibition (85) and are therefore likely contributors to inhibition of filamentous growth in the zebrafish host. The increased hyphal growth in p47^{phox} morphants, in which *C. albicans* does not appear to be under oxidative stress, clarifies conflicting *in vitro* observations. It suggests that during infection, host-derived reactive oxygen species tend to inhibit (15) rather than activate (24, 59) the yeast-hypha switch. NADPH oxidase-generated reactive oxygen and nitrogen species may directly inhibit filamentation (6). Other, more recently described responses that require this enzyme complex may also be involved, including alteration of the phagosomal redox state (72), modulation of phagosomal ion concentrations (74), inhibition of phagocyte inflammatory responses (58, 69, 75), and neutrophil extracellular trap production (10). It will be informative to combine morpholino-mediated gene knockdown and *in vivo* visualization in the zebrafish larva to determine which NADPH oxidase-dependent mechanism(s) is required to inhibit filamentation *in vivo*.

Our findings of heterogeneous levels of *CTA1* promoter activity, obtained using noninvasive *in vivo* imaging, provide complementary data to those of Brown and colleagues (31), who imaged the *CTA1-GFP* reporter strain in fixed histological sections from mice with disseminated candidiasis. Time-lapse studies with fluorescently marked immune cells in zebrafish, combined with morpholino-mediated gene knockdown, could address both the molecular basis for heterogeneity in observed oxidative stress *in vivo* and its direct consequences on fungal morphogenesis.

The mammalian host is endothermic, with normal temperatures of 36.8 ± 0.4°C for humans (55) and activity-dependent temperatures for mice of 36 to 37°C, with occasional dips in body temperature down to 28°C (73). Zebrafish grow at a wide range of temperatures, from 22 to 33°C, and ideally at 28°C (83). This difference in host temperature may be less of an issue for organisms such as *C. albicans* that grow and are pathogenic at a range of temperatures (34). Notably, although filamentous growth of *C. albicans* is enhanced at higher temperatures, we and others have observed fungal germination *in vivo* at 28°C and have implicated a role of filamentation in virulence in model hosts living at 28°C (14, 18, 19, 64). Furthermore, the intrinsic capacity of *C. albicans* to germinate within fish is apparently quite strong, because we found extensive filamentation upon reduction of phagocyte NADPH oxidase activity. In addition, preliminary results suggest that infected larvae maintained at 33°C versus 28°C have no major differences in *C. albicans* morphogenesis, fungal load, or fish mortality (data not shown). Taken together, these data suggest that despite the lower infection temperature, there is still good conservation of virulence and immune mechanisms. In fact, because zebrafish are ectothermic and can grow at temperatures between 18°C and 33°C, this model offers a unique opportunity to independently test the role of temperature in controlling *C. albicans* morphogenesis and virulence *in vivo*.

This novel model is a promising new resource that will enable fine-scale dissection of molecular mechanisms that direct *Candida*-host interaction. As we demonstrate, intravital imaging combined with morpholino gene knockdown, transgenic fish lines, and unique pathogen reporter strains can yield new insights into long-standing questions of innate immunity to fungal infection.

ACKNOWLEDGMENTS

We thank Carol Kim, Steve Renshaw, Nathan Lawson, Neta Dean, Deborah Hogan, and Alistair Brown for contributing reagents; Mark Nilan for excellent fish care; the laboratories of Carol Kim and Clarissa Henry (University of Maine) for patient advice, use of their equipment, and comments on the manuscript; Remi Gratacap, Danielle Garsin, and Mike Lorenz for comments on the manuscript; Alexa Lindauer for drawing the schematic images; William Halteman for expert statistical advice; Shawn Walls for ImageJ assistance; Ryan Phennicie for technical assistance; and Andre Khalil for image analysis advice.

This work was supported in part by a MAFES research assistantship to K.M.B., MAFES hatch grant E08913-08 to R.T.W., and NIH/NCRR award P20RR016463 to R.T.W.

REFERENCES

1. **Alonso-Monge, R., et al.** 1999. Role of the mitogen-activated protein kinase Hog1p in morphogenesis and virulence of Candida albicans. J. Bacteriol. **181:**3058–3068.
2. **Amatruda, J. F., J. L. Shepard, H. M. Stern, and L. I. Zon.** 2002. Zebrafish as a cancer model system. Cancer Cell **1:**229–231.
3. **Arana, D. M., R. Alonso-Monge, C. Du, R. Calderone, and J. Pla.** 2007. Differential susceptibility of mitogen-activated protein kinase pathway mutants to oxidative-mediated killing by phagocytes in the fungal pathogen Candida albicans. Cell. Microbiol. **9:**1647–1659.

4. **Aratani, Y., et al.** 2002. Critical role of myeloperoxidase and nicotinamide adenine dinucleotide phosphate-oxidase in high-burden systemic infection of mice with Candida albicans. J. Infect. Dis. **185:**1833–1837.
5. **Ashman, R. B., et al.** 2004. Innate versus adaptive immunity in Candida albicans infection. Immunol. Cell Biol. **82:**196–204.
6. **Babior, B. M.** 2004. NADPH oxidase. Curr. Opin. Immunol. **16:**42–47.
7. **Babior, B. M.** 1999. NADPH oxidase: an update. Blood **93:**1464–1476.
8. **Balish, E., et al.** 2005. Susceptibility of germfree phagocyte oxidase- and nitric oxide synthase 2-deficient mice, defective in the production of reactive metabolites of both oxygen and nitrogen, to mucosal and systemic candidiasis of endogenous origin. Infect. Immun. **73:**1313–1320.
9. **Behnsen, J., et al.** 2007. Environmental dimensionality controls the interaction of phagocytes with the pathogenic fungi Aspergillus fumigatus and Candida albicans. PLoS Pathog. **3:**e13.
10. **Bianchi, M., et al.** 2009. Restoration of NET formation by gene therapy in CGD controls aspergillosis. Blood **114:**2619–2622.
11. **Bowman, T. V., and L. I. Zon.** 2010. Swimming into the future of drug discovery: in vivo chemical screens in zebrafish. ACS Chem. Biol. **5:**159–161.
12. **Brachmann, C. B., et al.** 1998. Designer deletion strains derived from Saccharomyces cerevisiae S288C: a useful set of strains and plasmids for PCR-mediated gene disruption and other applications. Yeast **14:**115–132.
13. **Brannon, M. K., et al.** 2009. Pseudomonas aeruginosa type III secretion system interacts with phagocytes to modulate systemic infection of zebrafish embryos. Cell. Microbiol. **11:**755–768.
14. **Brennan, M., D. Y. Thomas, M. Whiteway, and K. Kavanagh.** 2002. Correlation between virulence of Candida albicans mutants in mice and Galleria mellonella larvae. FEMS Immunol. Med. Microbiol. **34:**153–157.
15. **Brown, A. J., K. Haynes, and J. Quinn.** 2009. Nitrosative and oxidative stress responses in fungal pathogenicity. Curr. Opin. Microbiol. **12:**384–391.
16. **Calderone, R., and J. Sturtevant.** 1994. Macrophage interactions with Candida. Immunol. Ser. **60:**505–515.
17. **Carradice, D., and G. J. Lieschke.** 2008. Zebrafish in hematology: sushi or science? Blood **111:**3331–3342.
18. **Chamilos, G., et al.** 2006. Drosophila melanogaster as a facile model for large-scale studies of virulence mechanisms and antifungal drug efficacy in Candida species. J. Infect. Dis. **193:**1014–1022.
19. **Chao, C. C., et al.** 2010. Zebrafish as a model host for Candida albicans infection. Infect. Immun. **78:**2512–2521.
20. **Charlier, C., et al.** 2009. Evidence of a role for monocytes in dissemination and brain invasion by Cryptococcus neoformans. Infect. Immun. **77:**120–127.
21. **Chauhan, N., J. P. Latge, and R. Calderone.** 2006. Signalling and oxidant adaptation in Candida albicans and Aspergillus fumigatus. Nat. Rev. Microbiol. **4:**435–444.
22. **Clatworthy, A. E., et al.** 2009. Pseudomonas aeruginosa infection of zebrafish involves both host and pathogen determinants. Infect. Immun. **77:**1293.
23. **Clay, H., et al.** 2007. Dichotomous role of the macrophage in early Mycobacterium marinum infection of the zebrafish. Cell Host Microbe **2:**29–39.
24. **da Silva Dantas, A., et al.** 2010. Thioredoxin regulates multiple hydrogen peroxide-induced signaling pathways in Candida albicans. Mol. Cell. Biol. **30:**4550–4563.
25. **Davis, J. M., and L. Ramakrishnan.** 2009. The role of the granuloma in expansion and dissemination of early tuberculous infection. Cell **136:**37–49.
26. **de Repentigny, L.** 2004. Animal models in the analysis of Candida host-pathogen interactions. Curr. Opin. Microbiol. **7:**324–329.
27. **d'Ostiani, C. F., et al.** 2000. Dendritic cells discriminate between yeasts and hyphae of the fungus Candida albicans. Implications for initiation of T helper cell immunity in vitro and in vivo. J. Exp. Med. **191:**1661–1674.
28. **Drevets, D. A., P. J. Leenen, and R. A. Greenfield.** 2004. Invasion of the central nervous system by intracellular bacteria. Clin. Microbiol. Rev. **17:** 323–347.
29. **Eisen, J. S., and J. C. Smith.** 2008. Controlling morpholino experiments: don't stop making antisense. Development **135:**1735–1743.
30. **Ellett, F., L. Pase, J. W. Hayman, A. Andrianopoulos, and G. J. Lieschke.** 2011. mpeg1 promoter transgenes direct macrophage-lineage expression in zebrafish. Blood **117:**e49.
31. **Enjalbert, B., D. M. MacCallum, F. C. Odds, and A. J. Brown.** 2007. Niche-specific activation of the oxidative stress response by the pathogenic fungus Candida albicans. Infect. Immun. **75:**2143–2151.
32. **Ernst, J. F.** 2000. Transcription factors in Candida albicans—environmental control of morphogenesis. Microbiology **146:**1763.
33. **Frohner, I. E., C. Bourgeois, K. Yatsyk, O. Majer, and K. Kuchler.** 2009. Candida albicans cell surface superoxide dismutases degrade host-derived reactive oxygen species to escape innate immune surveillance. Mol. Microbiol. **71:**240–252.
34. **Fuchs, B. B., and E. Mylonakis.** 2006. Using non-mammalian hosts to study fungal virulence and host defense. Curr. Opin. Microbiol. **9:**346–351.
35. **Gietz, R. D., R. H. Schiestl, A. R. Willems, and R. A. Woods.** 1995. Studies on the transformation of intact yeast cells by the LiAc/SS-DNA/PEG procedure. Yeast **11:**355–360.
36. **Gray, C., et al.** 2011. Simultaneous intravital imaging of macrophage and neutrophil behaviour during inflammation using a novel transgenic zebrafish. Thromb. Haemost. **105:**105.
37. **Hall, C., M. V. Flores, T. Storm, K. Crosier, and P. Crosier.** 2007. The zebrafish lysozyme C promoter drives myeloid-specific expression in transgenic fish. BMC Dev. Biol. **7:**42.
38. **Hermann, A. C., and C. H. Kim.** 2005. Effects of arsenic on zebrafish innate immune system. Mar. Biotechnol. (New York) **7:**494–505.
39. **Ingham, P. W.** 2009. The power of the zebrafish for disease analysis. Hum. Mol. Genet. **18:**R107–R112.
40. **Keppler-Ross, S., C. Noffz, and N. Dean.** 2008. A new purple fluorescent color marker for genetic studies in Saccharomyces cerevisiae and Candida albicans. Genetics **179:**705–710.
41. **Kimmel, C. B., W. W. Ballard, S. R. Kimmel, B. Ullmann, and T. F. Schilling.** 1995. Stages of embryonic development of the zebrafish. Dev. Dyn. **203:**253–310.
42. **Kumamoto, C. A., and M. D. Vinces.** 2005. Contributions of hyphae and hypha-co-regulated genes to Candida albicans virulence. Cell. Microbiol. **7:**1546–1554.
43. **Lam, S. H., et al.** 2002. Morphologic transformation of the thymus in developing zebrafish. Dev. Dyn. **225:**87–94.
44. **Lavigne, L. M., et al.** 2007. Integrin engagement mediates the human polymorphonuclear leukocyte response to a fungal pathogen-associated molecular pattern. J. Immunol. **178:**7276–7282.
45. **Lawson, N. D., and B. M. Weinstein.** 2002. In vivo imaging of embryonic vascular development using transgenic zebrafish. Dev. Biol. **248:**307–318.
46. **Le Guyader, D., et al.** 2008. Origins and unconventional behavior of neutrophils in developing zebrafish. Blood **111:**132–141.
47. **Lehrer, R. I.** 1970. Measurement of candidacidal activity of specific leukocyte types in mixed cell populations. I. Normal, myeloperoxidase-deficient, and chronic granulomatous disease neutrophils. Infect. Immun. **2:**42–47.
48. **Lesley, R., and L. Ramakrishnan.** 2008. Insights into early mycobacterial pathogenesis from the zebrafish. Curr. Opin. Microbiol. **11:**277–283.
49. **Levraud, J. P., E. Colucci-Guyon, M. J. Redd, G. Lutfalla, and P. Herbomel.** 2008. In vivo analysis of zebrafish innate immunity. Methods Mol. Biol. **415:**337–363.
50. **Levraud, J. P., et al.** 2009. Real-time observation of Listeria monocytogenes-phagocyte interactions in living zebrafish larvae. Infect. Immun. **77:**3651.
51. **Lionakis, M. S., J. K. Lim, C. C. Lee, and P. M. Murphy.** 2010. Organ-specific innate immune responses in a mouse model of invasive candidiasis. J. Innate Immun. **3:**180–199.
52. **Lo, H. J., et al.** 1997. Nonfilamentous C. albicans mutants are avirulent. Cell **90:**939–949.
53. **Lorenz, M. C., J. A. Bender, and G. R. Fink.** 2004. Transcriptional response of Candida albicans upon internalization by macrophages. Eukaryot. Cell **3:**1076–1087.
54. **Lugo-Villarino, G., et al.** 2010. Identification of dendritic antigen-presenting cells in the zebrafish. Proc. Natl. Acad. Sci. U. S. A. **107:**15850–15855.
55. **Mackowiak, P. A., S. S. Wasserman, and M. M. Levine.** 1992. A critical appraisal of 98.6 F, the upper limit of the normal body temperature, and other legacies of Carl Reinhold August Wunderlich. JAMA **268:**1578.
56. **Meeker, N. D., and N. S. Trede.** 2008. Immunology and zebrafish: spawning new models of human disease. Dev. Comp. Immunol. **32:**745–757.
57. **Meijer, A. H., et al.** 2008. Identification and real-time imaging of a myc-expressing neutrophil population involved in inflammation and mycobacterial granuloma formation in zebrafish. Dev. Comp. Immunol. **32:**36–49.
58. **Morgenstern, D. E., M. A. Gifford, L. L. Li, C. M. Doerschuk, and M. C. Dinauer.** 1997. Absence of respiratory burst in X-linked chronic granulomatous disease mice leads to abnormalities in both host defense and inflammatory response to Aspergillus fumigatus. J. Exp. Med. **185:**207–218.
59. **Nasution, O., et al.** 2008. Hydrogen peroxide induces hyphal differentiation in Candida albicans. Eukaryot. Cell **7:**2008–2011.
60. **Newman, S. L., B. Bhugra, A. Holly, and R. E. Morris.** 2005. Enhanced killing of Candida albicans by human macrophages adherent to type 1 collagen matrices via induction of phagolysosomal fusion. Infect. Immun. **73:** 770–777.
61. **Nusslein-Volhard, C., and R. Dahm (ed.).** 2002. Zebrafish: a practical approach, vol. 261. Oxford University Press Inc., New York, NY.
62. **Pfaller, M. A., and D. J. Diekema.** 2007. Epidemiology of invasive candidiasis: a persistent public health problem. Clin. Microbiol. Rev. **20:**133–163.
63. **Prajsnar, T. K., V. T. Cunliffe, S. J. Foster, and S. A. Renshaw.** 2008. A novel vertebrate model of Staphylococcus aureus infection reveals phagocyte dependent resistance of zebrafish to non host specialized pathogens. Cell. Microbiol. **10:**2312–2325.
64. **Pukkila-Worley, R., A. Y. Peleg, E. Tampakakis, and E. Mylonakis.** 2009. Candida albicans hyphal formation and virulence assessed using a Caenorhabditis elegans infection model. Eukaryot. Cell **8:**1750–1758.
65. **Redd, M. J., G. Kelly, G. Dunn, M. Way, and P. Martin.** 2006. Imaging macrophage chemotaxis in vivo: studies of microtubule function in zebrafish wound inflammation. Cell Motil. Cytoskeleton **63:**415–422.
66. **Renshaw, S. A., et al.** 2006. A transgenic zebrafish model of neutrophilic inflammation. Blood **108:**3976–3978.
67. **Riggle, P. J., K. A. Andrutis, X. Chen, S. R. Tzipori, and C. A. Kumamoto.** 1999. Invasive lesions containing filamentous forms produced by a Candida

albicans mutant that is defective in filamentous growth in culture. Infect. Immun. **67:**3649–3652.
68. **Rogers, T. J., and E. Balish.** 1980. Immunity to Candida albicans. Microbiol. Rev. **44:**660–682.
69. **Romani, L., et al.** 2008. Defective tryptophan catabolism underlies inflammation in mouse chronic granulomatous disease. Nature **451:**211–215.
70. **Rozell, B., P. O. Ljungdahl, and P. Martinez.** 2006. Host-pathogen interactions and the pathological consequences of acute systemic Candida albicans infections in mice. Curr. Drug Targets **7:**483–494.
71. **Rubin-Bejerano, I., I. Fraser, P. Grisafi, and G. R. Fink.** 2003. Phagocytosis by neutrophils induces an amino acid deprivation response in Saccharomyces cerevisiae and Candida albicans. Proc. Natl. Acad. Sci. U. S. A. **100:**11007–11012.
72. **Rybicka, J. M., D. R. Balce, M. F. Khan, R. M. Krohn, and R. M. Yates.** 2010. NADPH oxidase activity controls phagosomal proteolysis in macrophages through modulation of the lumenal redox environment of phagosomes. Proc. Natl. Acad. Sci. U. S. A. **107:**10496–10501.
73. **Schubert, K. A., et al.** 2010. Daily torpor in mice: high foraging costs trigger energy-saving hypothermia. Biol. Lett. **6:**132.
74. **Segal, A. W.** 2005. How neutrophils kill microbes. Annu. Rev. Immunol. **23:**197–223.
75. **Segal, B. H., et al.** 2010. NADPH oxidase limits innate immune responses in the lungs in mice. PLoS One **5:**e9631.
76. **Seider, K., A. Heyken, A. Luttich, P. Miramon, and B. Hube.** 2010. Interaction of pathogenic yeasts with phagocytes: survival, persistence and escape. Curr. Opin. Microbiol. **13:**1–9.
77. **Shen, J., W. Guo, and J. R. Kohler.** 2005. CaNAT1, a heterologous dominant selectable marker for transformation of Candida albicans and other pathogenic Candida species. Infect. Immun. **73:**1239–1242.
78. **Sullivan, C., and C. H. Kim.** 2008. Zebrafish as a model for infectious disease and immune function. Fish Shellfish Immunol. **25:**341–350.
79. **Tobin, D. M., et al.** 2010. The lta4h locus modulates susceptibility to mycobacterial infection in zebrafish and humans. Cell **140:**717–730.
80. **Van Der Sar, A. M., et al.** 2003. Zebrafish embryos as a model host for the real time analysis of Salmonella typhimurium infections. Cell. Microbiol. **5:**601–611.
81. **Vergunst, A. C., A. H. Meijer, S. A. Renshaw, and D. O'Callaghan.** 2010. Burkholderia cenocepacia creates an intramacrophage replication niche in zebrafish embryos, followed by bacterial dissemination and establishment of systemic infection. Infect. Immun. **78:**1495.
82. **Walters, K. B., J. M. Green, J. C. Surfus, S. K. Yoo, and A. Huttenlocher.** 2010. Live imaging of neutrophil motility in a zebrafish model of WHIM syndrome. Blood **116:**2803–2811.
83. **Westerfield, M.** 2000. The zebrafish book. A guide for the laboratory use of zebrafish (Danio rerio). University of Oregon Press, Eugene, OR.
84. **Wheeler, R. T., D. Kombe, S. D. Agarwala, and G. R. Fink.** 2008. Dynamic, morphotype-specific Candida albicans beta-glucan exposure during infection and drug treatment. PLoS Pathog. **4:**e1000227.
85. **Wozniok, I., et al.** 2008. Induction of ERK-kinase signalling triggers morphotype-specific killing of Candida albicans filaments by human neutrophils. Cell. Microbiol. **10:**807–820.
86. **Wu, L., and V. N. KewalRamani.** 2006. Dendritic-cell interactions with HIV: infection and viral dissemination. Nat. Rev. Immunol. **6:**859–868.
87. **Zapata, A., B. Diez, T. Cejalvo, C. Gutierrez-de Frias, and A. Cortes.** 2006. Ontogeny of the immune system of fish. Fish Shellfish Immunol. **20:**126–136.